Tailoring Organic-Organic Poly(vinylpyrrolidone) Microparticles and Fibers with Multi-Walled Carbon Nanotubes for Reinforced Composites

Christian P. Narvaez-Muñoz,*,† Luis M. Carrion-Matamoros,† Karla Vizuete,‡ Alexis Debut,‡ Carlos R. Arroyo,‡ Víctor Guerrero,¶ Cristina E. Almeida-Naranjo,¶ Víctor Morales-Flórez,§ Duncan J. Mowbray,‖ and Camilo Zamora-Ledezma*,‖,⊥

‖School of Physical Sciences and Nanotechnology, Yachay Tech University, 100119-Urcuquí, Ecuador
†Laboratorio de Reologia y Fluidos Complejos, Universidad de las Fuerzas Armadas (ESPE), Sangolquí, Ecuador
‡Centro de Nanociencia y Nanotecnología, Universidad de las Fuerzas Armadas (ESPE), Sangolquí, Ecuador
¶Escuela Politécnica Nacional, Departamento de Materiales, Quito, Ecuador
§Departamento de Física de la Materia Condensada, Universidad de Sevilla, Avenida Reina Mercedes, 41012 Seville, Spain
⊥Instituto Venezolano de Investigaciones Científicas (IVIC), Apartado 20632, Caracas 1020-A, Venezuela

ABSTRACT: Polymeric-based microparticles and fibers are tailorable for a wide range of common industrial and biomedical applications, while multi-walled carbon nanotubes (MWCNTs) are among the most useful macromolecules based on their outstanding electronic, mechanical, and optical properties at the nanoscale. By combining these nanostructures with various polymeric precursors, their range of potential applications becomes even greater. One of the simplest and most affordable methods for fabricating micro and nanostructures is electrospinning. Herein we demonstrate how MWCNTs may be used to produce tailor-made organic-organic poly(vinylpyrrolidone) (PVP) microparticles and fibers via electrospinning by studying their structural, vibrational, rheological and mechanical properties' dependence on their solvent (ethanol (EtOH) or dimethylformamide (DMF)) and resulting morphology. Specifically, we find clear differences in morphologies from perfectly spherical and isolated microparticles to fibers mats, or a combination of fibers with entangled beads, with solvent type and concentration. Based on our findings, we propose that the mechanism governing the shape and size of the particles is a competition between the solvent's surface tension, dielectric constant and viscoelastic properties. We show, based on both our experimental results and density functional theory (DFT) calculations, that OH-functionalization of the MWCNTs is essential for achieving high PVP coverages and promoting the stability of the resulting PVP/MWCNT nanocomposite. Finally, by fabricating PVP/MWCNT fiber mats, we demonstrate that low concentrations (0.01 to 0.1 wt.%) of MWCNTs lead to a qualitative improvement (~ 250 %) in the resulting mechanical properties, i.e., a reinforced composite. These results show how by controlling the solvent's dielectric constant, surface tension, and concentration one may produce tailor-made PVP nanomaterials in combination with other organic/inorganic nanoparticles, i.e., silver, gold, or carbon allotropes, for next-generation applications.

KEYWORDS: PVP • DMF • ethanol • MWCNT • rheology • Raman • DFT • mechanical reinforcement

1. INTRODUCTION

Tailor-made polymeric-based particles or fibers in the micro/nano range are suitable for a wide range of everyday applications. These include polymer-assisted synthesis of functional nanostructures for the pharmaceutical, cosmetic and food industry , while fibers and fiber-mats have been effectively used as filters for water remediation and biomedical applications[1,2]. Many of these applications require not only the modulation of the shape and size of the nanoparticles, but also their internal morphology and roughness. For instance, porous microparticles or fibers have been widely used for both sequestration of targeted molecules and as multifunctional material templates.[3] When these polymeric based micro/nanostructures are combined with different functional macromolecules or nanoparticles, their potential is even greater.[4–10]

Some of the most commonly used macromolecules are multi-walled carbon nanotubes (MWCNTs) due to their intrinsic properties at the nanoscale, e.g., ballistic conductivity, high tensile strength, and nearly one dimensional nature[11]. However, to exploit these properties at the macroscopic scale, one must ensure a nearly homogeneous dispersion of the macromolecule during composite processing. Recently, considerable attention has been paid to developing and refining existing techniques and methods to affordably produce particles with a controlled morphology. With this aim, the electrohydrodynamic atomization (EHDA) technique, commonly

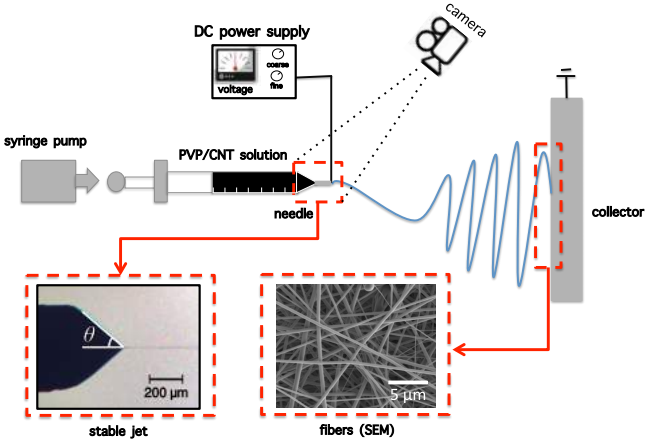

Figure 1. Schematic of the electrospray setup, with the half angle θ of the Taylor cone for a stable jet and a SEM image of fibers shown as insets.

known as electrospinning, has been frequently used to produce particles ranging from the micro to nanoscale [2,12]. Although this technique has been studied for more than a century, only recently has it been successfully applied to fabricate a wide range of custom made micro and nanostructured materials. [1,2,12,13] It is worth noting that a shortcoming of electrospinning is its unsuitability for the mass-production of nanofibers. However, this may be overcome through the use of modified technologies, such as bubble electrospinning. [14]

The electrospinning technique, depicted schematically in Figure 1, consists of atomizing a conductive solution into a spray of fine droplets by applying a strong electric field. The stabilization of the electrospray process occurs when the electrostatic forces overcome the surface tension of the liquid. As the voltage increases, the multiple expelling jets can be modulated. However, most applications are focused on the stable or cone-jet regime, which is the simplest and most reliable mode for the production of microparticles and fibers. [15,16] Figure 1 shows a classic optical micrograph of the Taylor cone, the definition of the half-angle cone for a stable jet, and also a scanning electron microscopy (SEM) image of a representative polymer-based fiber. Typically, a conductive liquid is pumped at a given flow rate through a capillary tube. A DC voltage is then applied between the liquid and a counter electrode or collector, which is usually flat and located at some distance from the syringe needle. Due to the electrostatic forces, the solution is expelled from the end of the capillary tube forming a spray of small droplets, which are deposited on the collector.

Several experimental and theoretical investigations have focused on possible applications of polymer particles fabricated through the electrospray technique [1,2,15]. Polymers with high molecular weight usually produce higher viscosity conductive solutions and are often used to produce fibers. [16] Several precursors, e.g., polylactic-co-glycolic acid (PLGA), polylactic acid (PLA), polyvinylpyrrolidone (PVP), poly caprolactone (PCL) and polymethyl methacrylate (PMMA), have been widely used to fabricate micro and nanoparticles through this technique. Among the most versatile polymers used so far, PVP deserves special attention mainly due to its biocompatibility. Specifically, PVP has been approved by the American Food and Drug Administration for applications in the medical and pharmaceutical industries. [12]

For these reasons, we focus herein on the tailoring of PVP microparticles and fibers with MWCNTs by varying the PVP concentration when using ethanol (EtOH) or dimethylformamide (DMF) as a solvent. We provide a phase diagram analyzing the effect of the solvent's dielectric constant and viscosity on the resulting micro/nano structures, and provide an overview of the processes involved for making tailored PVP microparticle and nanofiber mats. These results are elucidated via our proposed mechanism for governing the micro/nano structure of the composite. We clarify the essential role played by OH-functionalization of carbon fillers for achieving stable PVP/MWCNT colloidal solutions based on our experimental measurements and DFT calculations. Finally, we demonstrate that at very low concentrations MWCNTs can be employed for mechanical reinforcement of the resulting PVP/MWCNT mats, i.e., a reinforced composite.

2. MATERIALS AND METHODS

2.1. Materials. Polyvinylpyrrolidone (PVP) K30 (molecular weight 27000 ~ 32400 g/mol) was purchased from Yuking (Shanghai, China). Dimethylformamide (DMF) and ethanol (EtOH) ≥ 99.5% analytical grade was acquired from Fisher Scientific (Cali, Colombia) and PanReac Laboratory, respectively.

OH-functionalized multi-walled carbon nanotubes (MWCNTs) were purchased from Nanostructured & Amorphous Materials, Inc., with purity > 95%, short length $L \approx 2.5$ μm, inner diameter $d_{inner} \approx 4 \pm 1$ nm, outer diameter $d_{out} \approx 11.5 \pm 3.5$ nm, specific surface area $A > 233$ m^2/g, bulk density $\rho_{bulk} \approx 0.39 \pm 0.03$ g/cm^3. Figures S1, S2, and S3 in the Supporting Information (SI) show a representative MWCNT powder's x-ray diffraction (XRD) pattern, scanning electron microscopy (SEM) and transmission electron microscopy (TEM) micrographs, respectively.

2.2. Microparticle and Fiber Fabrication. The starting material for all spherical microparticles and fibers was either conductive PVP or PVP/MWCNT solutions. For PVP particles/fibers a set of solutions with different PVP contents in DMF or EtOH was prepared. In a classic procedure, we poured the solvent into a beaker and then added a specific amount of PVP between 10 and 30 wt.%. Finally, the mixture was magnetically stirred at room temperature for 60 minutes until a light yellow homogeneous PVP/DMF or PVP/EtOH solution was obtained. Figure S4(a) in the SI shows a representative vial containing 5 mL of a homogeneous PVP/EtOH solution containing 30 wt.% PVP.

PVP/MWCNT fibers were fabricated employing selected parameters, i.e., EtOH as the solvent and 30 wt.% PVP. In this case, a typical procedure for producing a conductive solution containing the polymer precursor and the nanotubes was carried out in two steps. First, a 30 wt.% PVP/EtOH solution was prepared following the preceding protocol. This PVP mixture was then poured into a vial, afterwhich a specific amount of MWCNT powder was added from 0.01 to 0.2 wt.%. The PVP/MWCNT suspensions were homogenized by tip-sonication with a SONOPULS mini20 sonifier equipped with a 2.5 mm microtip operating at 75 kHz, which delivered pulses of 0.5 s separated by 1 s rest intervals. The ultrasonic nominal output maximum was fixed at 20 W. The sonication time was fixed at 60 minutes until a dark and homogeneous solution was obtained. All the samples were kept in an ice bath during sonication in order to avoid sample overheating, which in turn promotes polymer desorption from the nanotube surface and induces nanotube aggregation. Figure S4(b-d) in the SI shows representative vials containing 5 mL of a PVP/MWCNT homogeneous suspensions at different nanotube contents between 0.01 and 0.2 wt.%. The samples were entirely stable for several weeks.

2.3. Electrospray Experimental Setup. In the present work, microparticles and fibers were fabricated using the homemade electrospray setup depicted schematically in Figure 1. This configuration includes a high voltage source (Genvolt, model 73030, 30 kV) a syringe pump (Cole Palmer model 788110C), a spray head and a collector plate, allowing us to modulate the flow rate, the applied voltage, and the collecting distance. In a typical procedure, the conductive solution was poured into a 10 mL plastic syringe (NIPRO). The flow rate of the solution was controlled through the syringe pump and a stainless steel needle with a 0.4 mm internal diameter to produce the stable jet shown as an inset in Figure 1. These parameters were optimized by exploring flow rates between 0.1 and 0.4 mL/h and applied voltages between 7.5 and 12 kV as provided in Tables S1 and S2 of the SI. The Taylor cone was observed with an analogue charge coupled device (CCD) camera and IC Capture software. The particles produced were then deposited on an aluminum collector located at a distance between 12 and 14 cm from the needle tip. In order to determinate the optimal coverage, the collection time was varied from 30 seconds to 5 minutes. All electrospray processes were carried out at room temperature with a relative humidity of 48%. The optimal parameters used for our samples were a flow rate 0.1 mL/h and a collecting distance of 12 cm with the applied voltage adjusted slightly for each concentration.

2.4. Scanning Electron Microscopy (SEM). The size and morphology of our structures were characterized using a field-emission gun scanning electron microscope (FEG-SEM, Mira3

Tescan). Samples were directly deposited on aluminum sample-holders. The operation voltage ranged between 3 and 5 kV. In a classic procedure, low magnification (×2000) micrographs were obtained to determine the size distribution and higher magnification (×10000) micrographs were examined to obtain a refined description of the morphology of the particles. With this aim, samples were coated with a conducting gold layer of approximately 20 nm thickness using a sputtering evaporator (Quorum Q150 ES). A statistical analysis of the particles and fiber diameter distributions was carried out using the ImageJ software.[17]

2.5. Rheology. Rheological measurements were carried out employing a Discovery HR-2 from TA Instrument with a maximum angular velocity of 300 rad/s and torque of 0.2 N·m, with a torque resolution of 1×10^{-4} N·m. For the analysis, the configuration of concentric cylinders geometry was used. To prevent the sample drying, which in turn promotes a layer that hinders the measurement, a solvent trap based on hydrocarbon was prepared. A classic procedure for performing the measurements involves first a preshear during 10 s at a constant shear rate of 300 s^{-1}. This step was carried out in order to guarantee that the sample was homogeneously distributed throughout the geometry and to establish a uniform rheological condition, i.e., to replace any residual stress on the sample. Subsequently, a rest period was set at 300 s prior to the test in order to allow the fluid to reach the equilibrium within the geometry, and finally a steady flow study was carried out by means of a logarithmic scan at shear rates of 0.01 to 300 s^{-1} with a maximum equilibrium time of 200 s and a minimum of 5 s. All rheological measurements were made at room temperature. The rheological behavior of the system is explored through typical plots of viscosity and stress versus shear rate.

2.6. Raman. Raman spectra were recorded using a Horiba LabRAM HR evolution Raman spectrometer coupled with a CCD camera and excited by a solid-state red laser line (λ_{exc} = 633 nm) and equipped with a microscope configuration. Our measurements were carried out using a 100× objective lens, a laser spot size of about 0.5 μm to focus on the sample, and a spectral resolution of 0.35 cm^{-1}. The power density was kept below 50 mW in order to avoid sample overheating effects. Prior to usage, the spectrometer was calibrated using a silicon wafer's associated peak intensity located at 521 cm^{-1}. Spectra were recorded in the 200 to 3500 cm^{-1} region with a 1800 g/mm grating. In a typical procedure, the recording time was between 10 and 1000 s depending on the intensity of the signal, and two accumulations per spectrum segment were averaged. All Raman measurements were made at room temperature.

2.7. Mechanical Measurements. Tensile experiments were carried out at room temperature, employing a Discovery HR-2 from TA Instrument equipped with a dynamic mechanical analysis (DMA) accessory specially adapted for testing solid and soft-solid materials. This equipment can exert a maximum stress $\sigma \approx 80$ MPa, with stress and displacement resolutions of 0.008 MPa and 20 nm, respectively. In Figure S5 of the SI we show a photograph of this experimental setup. Measurements of at least three specimens for each sample were performed. The specimens were tested as yarns of diameter $d_y \approx 900$ μm and length $L \approx 3.0$ cm by rolling flat fiber mats. Sample widths and gauge lengths were measured using a digital caliper. Elastic modulii were obtained from a linear fit to the initial linear loading region of the stress-strain curves with root mean square errors $R^2 > 0.9$.

2.8. Computational Details. All density functional theory (DFT) calculations were performed using linear combinations of atomic orbitals (LCAOs)[18] from double-ζ-polarized (DZP) basis sets within the projector augmented wave (PAW) method[19] code GPAW.[20] The generalized gradient approximation (GGA), as implemented by Perdew, Burke, and Ernzerhof (PBE),[21] was employed for the exchange and correlation (xc) functional. We used a grid spacing of $h \approx 0.2$ Å and fully relaxed all atomic structures until a maximum force $\lesssim 0.03$ eV/Å was obtained using the atomic simulation environment (ASE) code.

To model the relative stability of EtOH and PVP on the pristine and OH-functionalized large diameter nanotubes ($d_{out} \approx 11.5$ nm) studied herein, we have employed a graphene model, neglecting curvature and interlayer contributions to the adsorption energies. A 2×5 repetition of the orthogonal graphene unit cell ($4.9924 \times 21.3146 \times 28.8$ $Å^3$) with $a \approx 4.651$ a_0 and a $7 \times 2 \times 1$ k-point sampling were employed for calculations of EtOH and PVP on pristine graphene (Gr) and hydroxide (OH) functionalized graphene (GrOH). This resulted in more than 20 Å of vacuum orthogonal to the graphene plane, and more than 10 Å separating PVP adsorbates. PVP was modeled as an infinite chain, with isolated PVP having a relaxed 4.6 Å unit cell parameter along the periodic direction. To quantify the charge transfer between EtOH or PVP and Gr or GrOH, we performed a Bader analysis[22] based on the all-electron charge density calculated with the PAW method in GPAW.[20]

The binding energy, E_{bind}, of an adsorbate $X \in \{\text{EtOH}, \text{PVP}\}$ on a given substrate $G \in \{\text{Gr}, \text{GrOH}\}$ is obtained from the difference in energy between the separated and combined systems, so that

$$E_{bind}[X@G] \approx E[X] + E[G] - E[X@G]. \quad (1)$$

Since we find EtOH and PVP do not form covalent bonds with Gr or GrOH, we may safely neglect any difference in entropy between the adsorbed and gas phase species, i.e., $\Delta S = S[X] + S[G] - S[X@G] \approx 0$. The ratio of forward to backward rate constants for the adsorption process $X + G \leftrightharpoons X@G$, $K[X@G] = k_+/k_-$, at temperature T is then[23–25]

$$K[X@G] \approx \exp\left(\frac{E_{bind}[X@G]}{k_B T}\right). \quad (2)$$

If we assume our system is in thermodynamic equilibrium, the coverage Θ of PVP and EtOH on Gr or GrOH depends on the concentration C in solution and the ratio of forward to backward rate

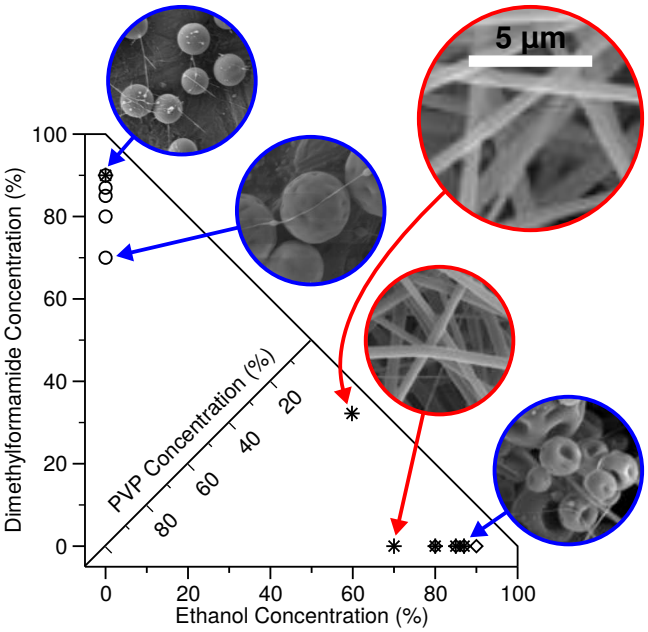

Figure 2. Phase diagram of dimethylformamide versus ethanol and PVP wt. % concentration for particles (circles), fibers (stars), and beads (diamonds). SEM images of fibers (red) and particles (blue) are shown as insets with a common 5 μm scale bar.

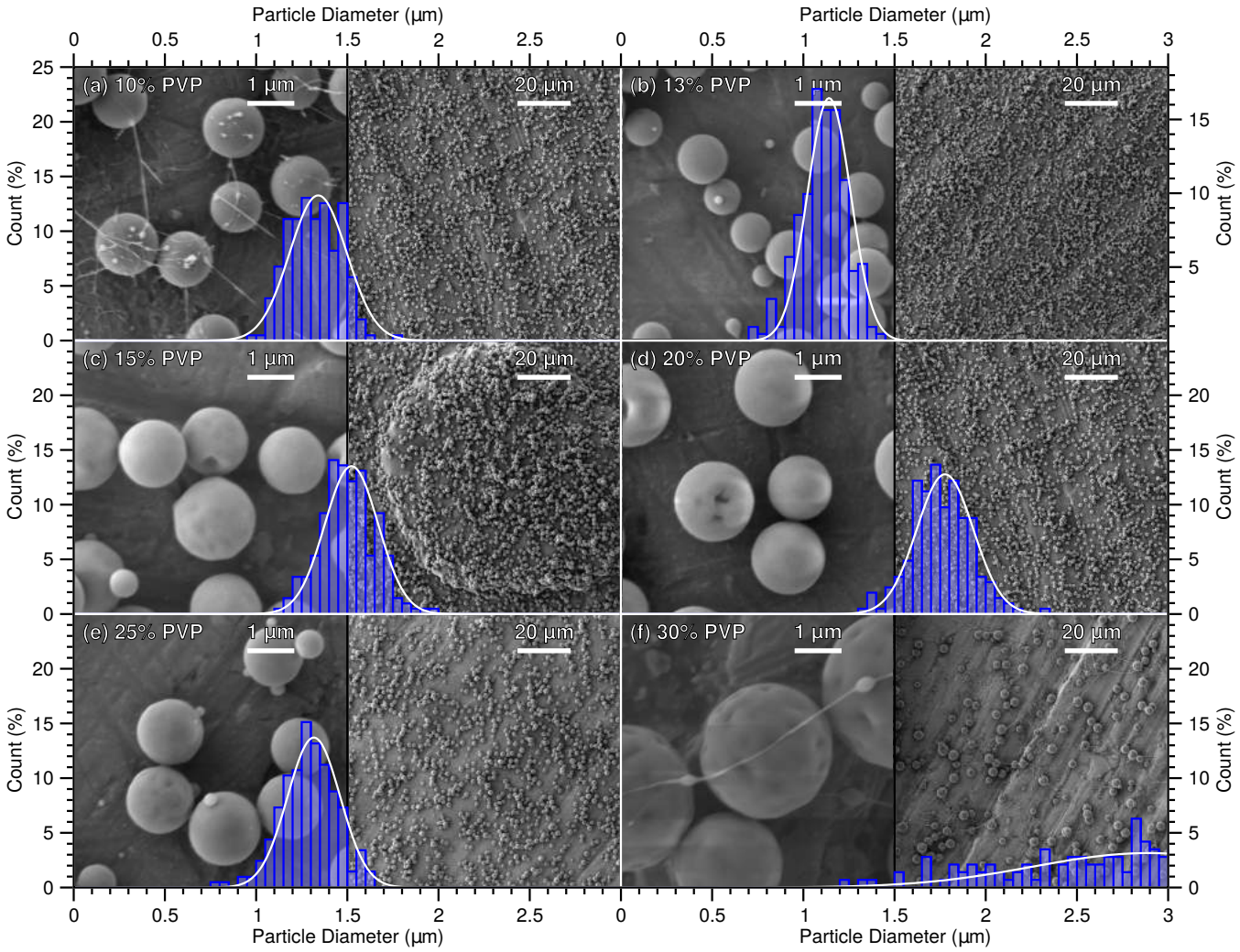

Figure 3. SEM images and particle diameter d_p (blue) distributions for PVP and dimethylformamide mixtures with PVP wt.% concentrations of (a) 10 ($d_p \approx 1.3 \pm 0.2$ μm), (b) 13 ($d_p \approx 1.1 \pm 0.1$ μm), (c) 15 ($d_p \approx 1.5 \pm 0.1$ μm), (d) 20 ($d_p \approx 1.8 \pm 0.2$ μm)), (e) 25 ($d_p \approx 1.3 \pm 0.1$ μm), and (f) 30 ($d_f \approx 2.9 \pm 0.6$ μm).

constants K for all adsorbates as follows:[23–25]

$$\Theta[X@G] \approx \frac{C[X]K[X@G]}{1 + \sum_{Y\in\{\mathrm{EtOH,PVP}\}} C[Y]K[Y@G]}. \quad (3)$$

Here, we obtain the fractional concentration C from the ratio of wt.% concentration in solution to the sum of atomic masses per unit cell, M[EtOH] = 70.091 and M[PVP] = 222.288 u/cell, normalized by their sum over all adsorbates in solution.

3. RESULTS AND DISCUSSION

3.1. Morphology Phase Diagram. A very useful tool for preparing nanocomposites is a phase diagram of nanocomposite morphology dependence on solvent concentration and type. Here we explore the PVP nanostructure dependence on DMF and EtOH concentration with the aim to produce tailored spherical microparticles and fibers, as summarized in the morphology phase diagram provided in Figure 2. By adjusting either the solvent or the viscoelastic properties of the solution used during electrospinning we may produce spherical microstructures with smooth surfaces, interconnected beads, beaded-fibers, or a single fiber mat. Most importantly, by employing a mixture of DMF and EtOH (65:35) we may obtain fiber mats with a significantly lower PVP concentration, as shown in Figure 2. This allows one to achieve significantly lower PVP to macromolecule or nanoparticle ratios, consequently widening the range of potential applications.

3.2. Scanning Electron Microscopy (SEM). The morphologies of the as-prepared composite fibers, with different solvents and weight ratios, were observed using a scanning electron microscope (SEM), as shown in Figures 3 and 4. Over each SEM image we have superimposed the histograms of the corresponding distribution of particle and fiber sizes, d_p and d_f, respectively. We first focus on those prepared with DMF (Figure 3), where we observe that DMF yields mainly microparticles, as expected from the literature[2,12,26]. At the same time it should be noted that the particle size increases with PVP concentration. For the extreme values (10 and 30 wt.% PVP concentration) we obtain nanosized connections between the majority of the microparticles. It is important to note that, beside the differences in particle sizes, in some cases the particles are almost perfectly spherical with a smooth surface, while in others, the particles have well defined pores (as for 30 wt.% PVP concentration). Features such as pores (or porous particles) are potential active sites for species adsorption in some applications.[2,12,26]

In contrast to the particles produced with DMF, when we use EtOH the microparticles are present in two distributions. One consists of larger sized particles whose size scales linearly with increasing PVP concentrations (Figure 4). The smaller diameter microparticles remain rather consistent in size up to a PVP concentration of 15 wt.%, afterwhich they are no longer present. To obtain a combination of fibers and particles we require a minimum PVP concentration of 13 wt.%. As the PVP concentration increases to 20 wt.%,

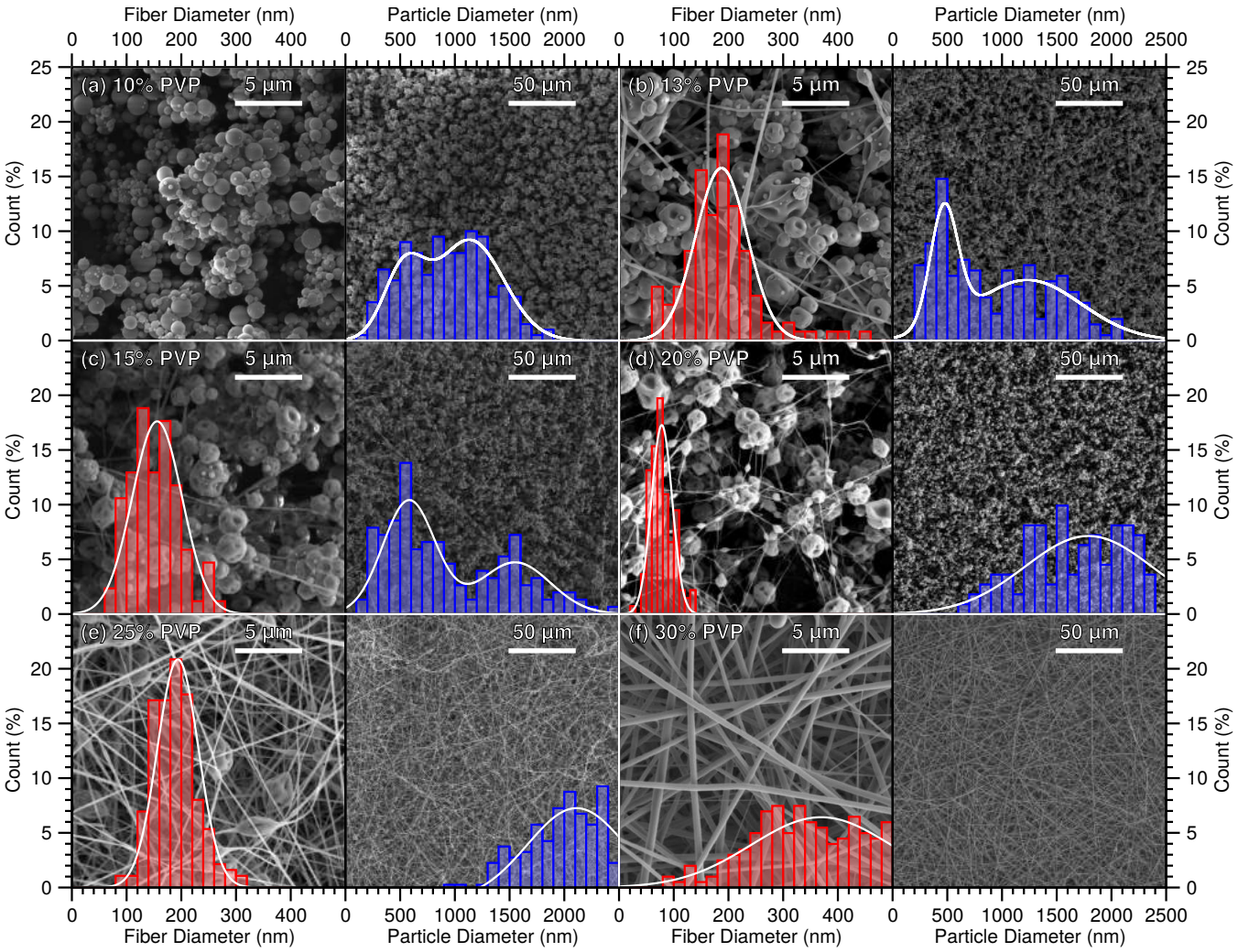

Figure 4. SEM images and fiber diameter d_f (red) and particle diameter d_p (blue) distributions for PVP and ethanol mixtures with PVP wt.% concentrations of (a) 10 ($d_p = 0.54 \pm 0.19$, 1.1 ± 0.3 µm), (b) 13 ($d_f \approx 0.17 \pm 0.05$, $d_p \approx 0.47 \pm 0.01$, 1.2 ± 0.5 µm), (c) 15 ($d_f \approx 0.16 \pm 0.05$, $d_p \approx 0.58 \pm 0.24$, 1.6 ± 0.3 µm), (d) 20 ($d_f \approx 78 \pm 19$ nm, $d_p \approx 1.8 \pm 0.6$ µm, (e) 25 ($d_f \approx 0.19 \pm 0.04$, $d_p \approx 2.1 \pm 0.5$ µm), and (f) 30 ($d_f \approx 0.37 \pm 0.13$ µm).

the fiber diameter decreases substantially from 170 nm to 78 nm, afterwhich it increases to 370 nm. At 10 wt.% PVP concentration, we have only beads with EtOH, while in the regime from 13 to 25 wt.% we have a combination of bead structures and fibers. As the PVP concentration increases, the ratio of particles to fibers shifts from a majority of particles for 13 wt.% to a majority of fibers for 25 wt.%. Finally, for a concentration of 30 wt.%, we obtain rather large diameter fiber mats, with a concomitantly larger size distribution. All these observation have been summarized in Figure 5, which shows the average particle (Figure 5(a,b)) and fiber (Figure 5(c)) size versus PVP % concentration for each nanocomposite.

3.3. Rheology. The viscoelastic properties for PVP solutions using DMF and EtOH as solvents were studied via rheological measurements. Figure S6 in the SI shows typical viscosity versus shear rate plots in the range of 0 to 300 s^{-1} for PVP solutions using either DMF or EtOH and various contents of polymer between 0 and 30 wt.% PVP. These results are summarized in Figure 6, which presents the viscosity versus PVP wt.% concentration in either DMF or EtOH for a fixed shear rate of 300 s^{-1}. We find that as the shear rate increases, the shear stress increases non-linearly, similar to a non-Newtonian fluid. Indeed, the viscosity also increases non-linearly as the polymer content increases for both DMF and EtOH solutions. Such behaviour demonstrates that these fluids behave as dilatant fluids or pseudoplastics.[27,28] It is important to note that PVP solutions with either solvent (DMF or EtOH) exhibit similar viscoelastic properties at the same PVP wt.% concentration, as shown in Figure 6. This represents a key parameter which must be taken into account when fabricating electrospun nanocomposites.

The particle/fiber morphology can be tuned by controlling not only the basic scaling of processing variables such as the electric current, voltage, and flow rate involved during electrospraying, but also by controlling the solution properties such as the charge density, dielectric constant, electrical conductivity, viscosity, boiling point, and surface tension.[26] In fact, many authors[1,2,12] claim that the morphology of polymer particles produced by electrospraying are complex functions of thermodynamic and kinetic effects. However, the general consensus is that in most cases the solvent properties are the major factors in determining the particle/fiber morphology.[1,2,12] With this in mind, we have employed two organic solvents (DMF/EtOH) with similar rheological properties but different dielectric constants of 38 and 24.5, respectively. The dielectric constant is a measure of the dipole moment and reflects the polarizability of the molecules.

The specific particle formation mechanism of electrosprayed conductive polymeric solutions can be explained through a competition between the polarizability or screening of the solvent and the viscosity for the PVP solution as the polymer content increases. On the one hand, the solvent's dielectric constant determines both the

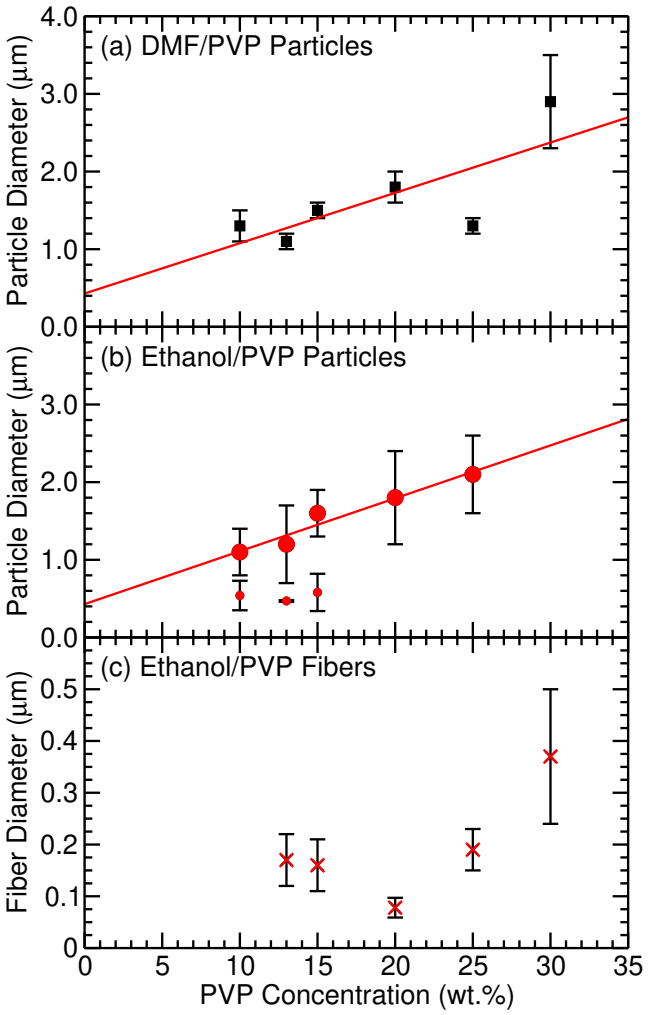

Figure 5. Average (a,b) particle (filled symbols) and (c) fiber (×) diameters d_p and d_f in μm, respectively, versus PVP wt.% concentration using (a) dimethylformamide (black squares) and (b,c) ethanol (red circles, ×) as solvents. Linear fits are shown in red as a guide to the eye. (b) Larger and smaller particle sizes are denoted by larger and smaller circles, respectively.

screening of the Coulombic repulsive force that drives the stretching of the charged jet and the electrostatic force that is responsible for carrying the charged jet to the collector. On the other hand, the viscosity of the PVP solution plays a crucial role in maintaining the stability of the cone jet during electrospinning that in turn modulates the particles/fibers morphology.

As reported for PVP polymer solutions[29], the particle size increases with increasing concentration in agreement with our findings (*cf.* Figure 5(a,b)). In addition, it has been reported[1,2,12] that an increase in boiling point is often correlated with a decrease in the particle size in concordance with our results, keeping in mind that the boiling point for DMF and EtOH are 153 and 78.5 °C respectively. Moreover, solvents with high boiling points (DMF) tend to produce mostly spherical shapes and smooth surfaces,[1,2,12] while solvents with lower boiling points (EtOH) tend to form beaded-fibers or fibers.

Regarding the viscoelastic effect on the particles' morphologies, our findings agree with those reported previously.[30] For EtOH, a transition from beaded structures for low viscosity polymer solutions through a biphasic region where beaded-fibers for medium viscosity system to a single fiber phase for high viscosity materials has been reported, analogous to the morphology phase diagram presented in Figure 2.

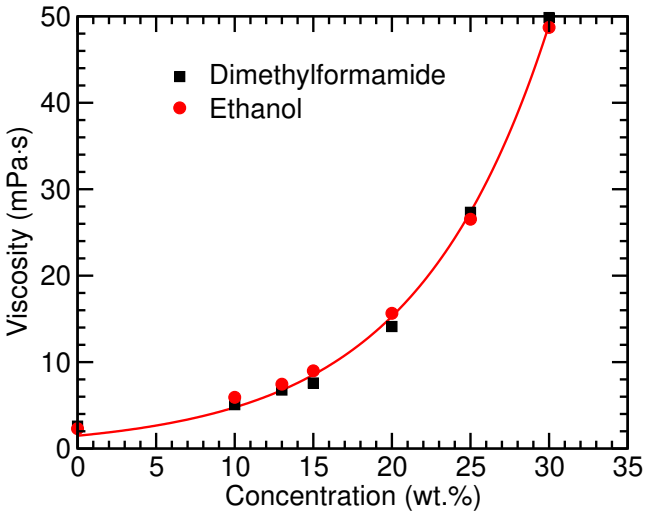

Figure 6. Viscosity in mPa·s or cP versus PVP wt.% concentration in dimethylformamide (black squares) or ethanol (red circles) for a shear rate of 300 s^{-1}.

Finally, it is worth mentioning that beaded-fibers were considered for many years to be a drawback of electrospun fibers. Recently, however, for many biotechnology applications controlling the bead morphology is now considered to be an asset for improving their final performance, e.g., for the fabrication of high performance filtering media[1,2,12].

3.4. Reinforced Composite. In order to exploit the potential applications of the PVP/MWCNT nanocomposites produced by the electrospinning method, we have fabricated a series of tailored beads/fibers using the optimal protocol provided by our morphology phase diagram (Figure 2). For beads, we were able to fabricate MWCNT beads using DMF as solvent with a polymer concentration of 13 wt.%. Similarly, we have prepared MWCNT fibers using EtOH as solvent and a polymer concentration of 30 wt.%. In both cases we kept the MWCNT content at 0.1 wt.%.

It is important to mention that, prior to deciding the "filler" to be used in the present work, we have performed several trials with two different sources of carbon nanotubes: (1) OH-functionalized MWCNTs from NanoAmor and (2) pristine single-walled carbon nanotubes (SWCNTs) from Elicarb. Figure S7(b-d) in the SI shows representative vials containing 5 mL of PVP/MWCNT homogeneous suspensions for various nanotube contents between 0.01 and 0.2 wt.%. We find the samples are entirely homogeneous and stable over several weeks. Figure S7(b-d) in the SI shows representative vials containing 5 mL of PVP/SWCNT mixtures for similar nanotube contents between 0.01 and 0.2 wt.%. In contrast to the PVP/MWCNT suspensions, the PVP/SWCNT samples are inhomogeneous and exhibit large agglomerates consisting mainly of SWCNT bundles. When we use these PVP/SWCNT conductive solutions in our electrospray set-up (Figure 1), we are unable to produce fibers or any other monodispersed nanostructure. However, when PVP/MWCNT suspensions are electrospun, homogeneous fiber mats are obtained.

In an effort to understand the chemical mechanism behind these observations, we have performed DFT calculations of EtOH and PVP adsorption on pristine (Gr) and OH-functionalized (GrOH) graphene, as depicted schematically in Figure 7. On the one hand, both EtOH and PVP physisorb on pristine graphene, with EtOH having a slightly stronger binding energy by 0.04 eV, as shown in Figure 7(a). As a result, at 10–30 wt.% PVP, the fractional coverage of Gr by PVP barely reaches 3% (*cf.* marked region of Figure 7(a)). This explains the poor dispersion we observe for pris-

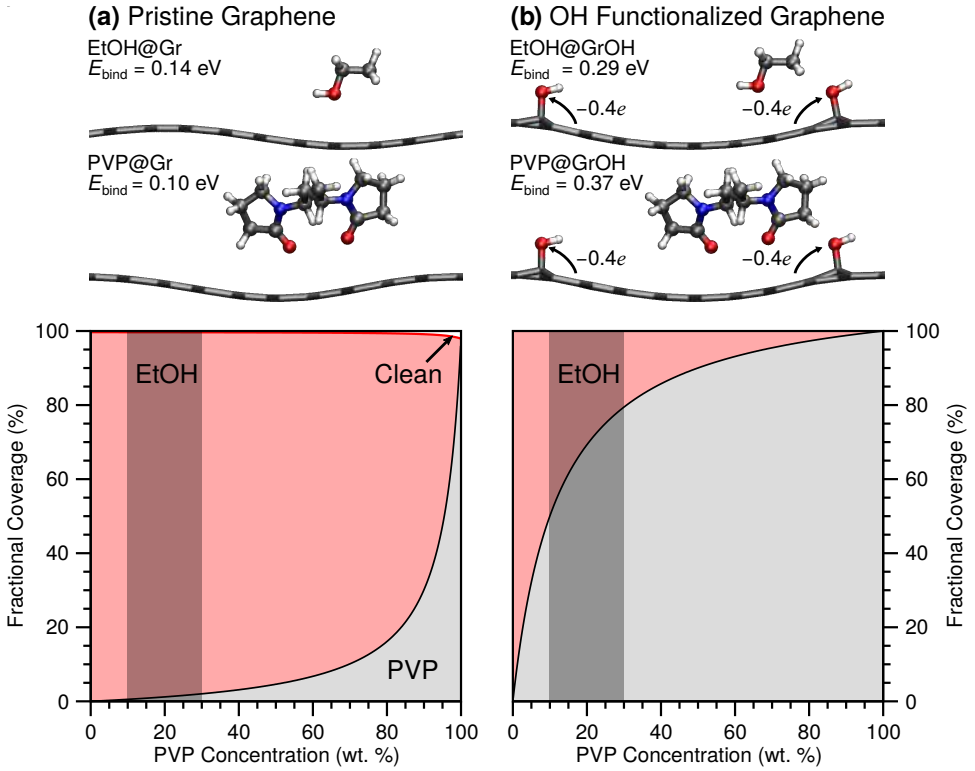

Figure 7. Binding energy E_{bind} in eV and fractional coverage Θ in % versus PVP concentration in wt.% of EtOH (red), PVP (grey), and empty sites (white) on (a) pristine graphene (Gr) and (b) OH-functionalized graphene (GrOH). Schematics of (a) EtOH@Gr, PVP@Gr, (b) EtOH@GrOH, and PVP@GrOH are provided as insets, with charge transfer within GrOH marked and C, N, O, and H atoms depicted in grey, blue, red, and white, respectively. The range of PVP concentrations in EtOH between 10 and 30 wt.% shown in Figure 3 is marked.

tine SWCNTs in PVP at $\lesssim$ 30 wt.%. On the other hand, whereas both EtOH and PVP exhibit a stronger binding on GrOH, PVP now has the stronger binding energy by 0.08 eV, as shown in Figure 7(b). For this reason, PVP already covers more than half of GrOH at concentrations of only 10 wt.% PVP, and reaches nearly 80% coverage at 30 wt.% PVP (*cf.* marked region of Figure 7(b)). This explains the stable homogeneous dispersions obtained for OH-functionalized PVP/MWCNTs.

It is important to note that the physisorption of both EtOH and PVP on GrOH is nearly isoenergetic when directly on the two OH adsorbates (not shown) or on the clean areas of the graphene substrate (see insets of Figure 7(b)). The role of the OH functionalization, rather than acting as active sites, instead seems to be withdrawing charge from the graphene layer, as we obtain a consistent charge transfer of $\sim$ 0.4 electrons to each OH adsorbate (*cf.* Figure 7(b)). For these reasons, we attribute the observed behavior to the affinity of the OH-functionalized MWCNTs' surface for promoting stabilization with PVP through its greater binding energy relative to EtOH.

As expected, these fibers exhibit similar features and morphologies to those produced without MWCNTs. Using these suspensions with MWCNT contents between 0.01 and 0.2 wt.% we have pre-

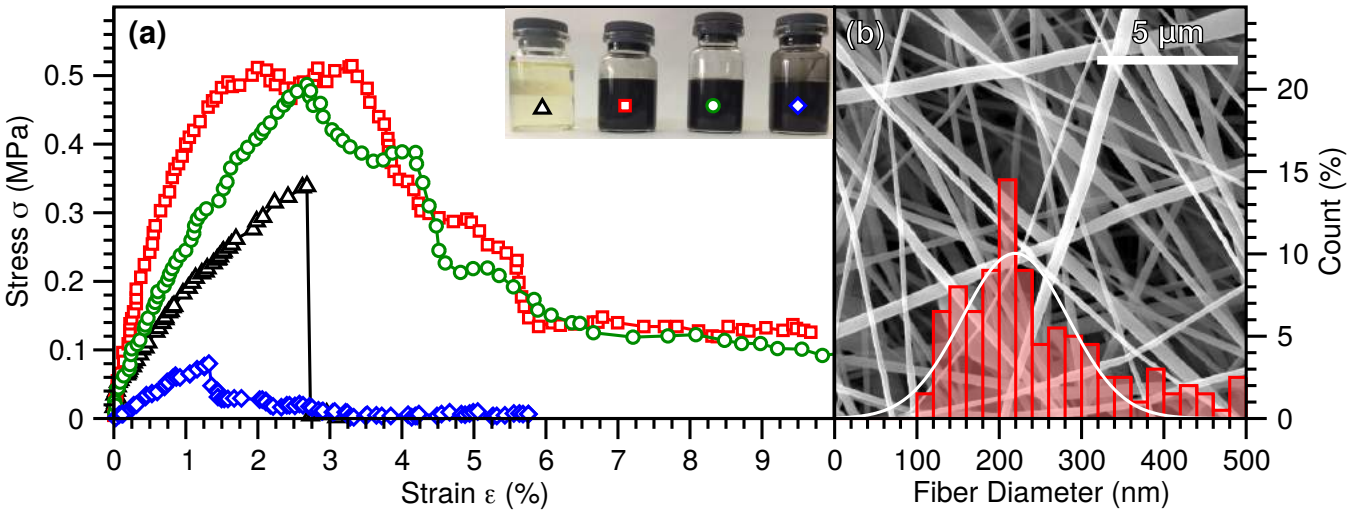

Figure 8. (a) Stress σ in MPa versus strain ε for tailored organic-organic PVP/MWCNT fiber samples with 10 wt.% PVP and 0 (black triangles), 0.01 (red squares), 0.1 (green circles), and 0.2 (blue diamonds) wt.% MWCNTs and (b) SEM images and fiber diameter d_f distribution for PVP/MWCNT hybrid materials with $d_f \approx 219 \pm 65$ nm. Vials containing 5 mL of each material are shown as an inset.

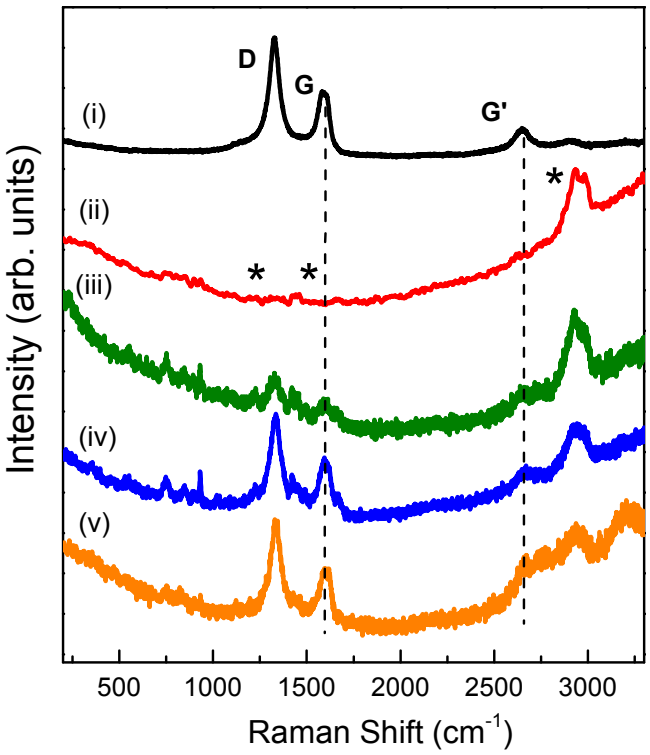

Figure 9. Raman spectra of (i) a multi-walled carbon nanotube (MWCNT) powder and (ii–iv) PVP/MWCNT nanocomposites consisting of 30 wt.% PVP and (ii) 0, (iii) 0.02, (iv) 0.2, and (v) 0.4 wt.% MWCNTs. All spectra were excited by a Nd:YAG red laser (λ_{exc} = 633 nm) and both normalized and shifted along the vertical axis for clarity. D, G, and G' bands and the relevant bands of PVP (*) are marked.

pared a set of macroscopic fiber-mats keeping the polymer content constant at 30 wt.%. This yields a final PVP/MWCNT mass ratio in the nanocomposites of 3000:1, 3000:10, and 3000:20. All these samples are homogeneous and exhibit mostly fibers with few beads. A representative SEM is shown in the background of Figure 8(b), corresponding to a sample containing a PVP/MWCNT ratio of (3000:20). The average fiber diameter in this fiber-mat is $d_f \approx 219 \pm 65$ nm, as shown in the histogram of Figure 8(b). The fiber diameter and its distribution are both significantly reduced relative to the pristine PVP 30 wt.% mats (*cf.* Figure 4(f)). By modulating the electrospinning parameters provided Table S2 of the SI, one may further reduce the diameter and its distribution, as extensively discussed in the literature.[12]

3.5. Raman. Raman spectroscopy is a powerful tool for the characterization of carbon-based nanocomposite materials. It provides valuable information about carbonaceous phases and their evolution throughout all the stages of material processing. Moreover, modern equipment offers a high spatial resolution, which is very important when analyzing nanocomposites for several applications[31]. Figure 9 shows typical Raman spectra of (i) MWCNT powder and (ii–iv) PVP/MWCNT fiber nanocomposites consisting of 30 wt.% PVP and 0 to 0.2 wt.% MWCNTs. The Raman spectrum for MWCNT powder exhibits typical fingerprints of NanoAmor–MWCNT: a flat spectrum accompanied by the main Raman peaks corresponding to the so-called defect, graphitic or second order (D, G, and G') bands located around 1350, 1590, and 2690 cm^{-1} respectively. These active Raman vibrational modes are attributable to: (1) disorder in graphitic materials (D band), (2) C–C in plane stretching modes (G-band), and (3) the second order harmonic of the D band (G'-band).[31] Conversely, the spectrum for 30 wt.% PVP (Figure 9(ii)) exhibits characteristic features of PVP:[31–33] a significant background attributable to the photoluminescent centers present in the composite,[10,34] with the occurrence of some peaks merging up from the continuum located as expected around 763, 1228, 1666, and 2930 cm^{-1}.[32,33] The low frequency modes are attributed to the C-N vibration band, while the weak and broad peak centered around 1666 cm^{-1} and the major peak located at 2930 cm^{-1} are ascribed to C=O and C-H stretching vibrations respectively.[32,33] As expected, for PVP/MWCNT fiber nanocomposites (Figure 9(iii,iv,v)), spectra show Raman fingerprints for MWCNTs, i.e. D, G, and G' bands, accompanied by a significant background attributable to organic impurities present in the nanocomposites. At the same time, the superimposed spectra exhibit characteristic features attributable to PVP. As the MWCNT content increases from 0.01, to 0.1 and finally 0.2 wt.% (Figure 9(iii,iv,v)), a clear trend in the spectra is observed. As the MWCNT content in the fiber mats increases, so does the graphitic Raman peak (G-band), while the peak intensity located at 2930 cm^{-1} and the photoluminescence attributed to PVP decrease accordingly. This result is in agreement with literature if we keep in mind that Raman spectroscopy in carbon nanotubes is a resonant process and so their signal should be much more intense than the non-resonant PVP signal. As we see in Figure 9, all Raman spectra for the organic-organic fiber nanocomposites exhibit similar features to those for nanotubes and the polymer precursor. This clearly indicates that the structure of the MWCNTs and PVP is conserved in the final composite.

3.6. Mechanical Properties. A very important physical parameter for nanocomposites is their mechanical response to an external force. Using the geometry for axial testing we have performed tensile tests on our PVP/MWCNT fiber yarns, subjecting them to a maximum stress of $\sigma \approx 80$ MPa. These measurements provide direct insight into the material's modulus of elasticity, or Young's Modulus (E), the yield strength, the tensile strength, and give us an overview of the homogeneity of the nanocomposite, allowing us to assess its potential applications. Figure 8 shows typical stress σ versus strain ε tests of PVP/MWCNT fiber nanocomposites consisting of 30 wt.% PVP and 0 to 0.2 wt.% MWCNTs. Our sample with the highest MWCNT concentration (0.2 wt.%) exhibits worse mechanical properties than the pure PVP nanocomposite. This saturation in improvement of mechanical properties with increasing CNT content is commonly observed in various CNT-based composites, such as ceramics, glasses, and hybrid nanofibers.[13,35] This is often attributed to poor CNT dispersion within the composite. Thus, by improving the CNTs' dispersion within the composite, greater mechanical reinforcement could be achieveable.

PVP fiber yarns without MWCNTs are quite fragile, with an initial elastic regime ($E = 12.8 \pm 0.2$ MPa) followed by a rupture below 3% strain at a tensile strength $\sigma_T \approx 0.34$ MPa, and showing no plastic regime. We find that the addition of only 0.01 wt.% MWCNTs increases the elastic modulus up to $E \approx 33 \pm 1$ MPa, ~ 250% higher than the samples without MWCNTs. Increasing the amount of MWCNTs does not yield stiffer samples, with the 0.10 wt.% sample exhibiting an elastic modulus of $E \approx 18 \pm 0.4$ MPa. Tensile strengths were also significantly increased (~ 50%) by the addition of MWCNTs to the fibers, achieving $\sigma_T \approx 0.51$ and 0.49 MPa with 0.01 and 0.10 wt.% MWCNTs, respectively.

This reinforcement through the addition of small amounts of CNTs has been previously reported for electrospun nylon fiber yarns,[36] where a 1.0 wt.% of CNTs increased the elastic modulus of the nylon from $E \approx 19.4$ to 28.0 MPa (≈ 46%) and the tensile strength from $\sigma_T \approx 10.45$ to 13.05 MPa (~ 25%). Moreover, instead of an extremely fragile rupture, we find the presence of the MWCNTs in the fibers produces a non-dramatic rupture processes. In all cases, samples broke below 16% strains, so clearly these materials are still quite fragile, and would not be good candidates for making

high tensile strength materials. For this reason, PVP is most often used to produce beads with specific functionalities rather than fibers [1,2,12]. However, these results provide a clear proof of concept for the mechanical reinforcement of organic-organic fibers, and suggest that even greater increases of the nanocomposite's mechanical properties could be attained by reducing the concentration of polymer further, e.g., by using a mixture of DMF and EtOH as solvents.

4. CONCLUSIONS

We have studied the fabrication of tailored organic-organic poly(vinylpyrrolidone) microparticles and fibers via electrospinning. We have mapped the resulting materials' morphology as a function of the solvent concentration for the preparation of micro beads and fibers based on PVP using DMF/EtOH. The resulting morphology phase diagram allows us to evaluate the solvent dependence of the micro/nano structures. Our results show that these parameters are critical to control not only the particle and fiber size and poly-dispersity, but also to induce changes on the particle's surface. For example, beads prepared from a PVP/DMF solution have a smooth flat surface for concentrations between 10 and 13 wt.%, afterwhich the surface's roughness increases with the PVP concentration, yielding porous beads at 30 wt.%. In this way, we obtain different morphologies from perfectly spherical and isolated micro/nano particles (beads) to fiber mats and an intermediate regime where a combination of fibers with entangled beads are produced. Based on our findings, the optimal parameters to produce tailor made particles or fibers for 13 wt.% PVP/DMF and 30% of PVP/EtOH, respectively, via the electrospray technique. We have discussed the mechanism that governs the particles micro and structures, and concluded that these differences in morphology and size can be attributed to a competition between the solvent's polarizability and the rheological properties of the PVP solutions. We have determined under which conditions fibers are grown for PVP/EtOH, allowing us to choose the optimal parameters to successfully fabricate mechanical reinforced tailored PVP/MWCNT bead/fiber nanocomposites by using different MWCNT concentrations for specific applications. Moreover, our combined experimental and DFT results clearly show that OH-functionalization of the MWCNTs is essential for achieving sufficiently high PVP coverages ($\sim 80\%$) to promote the stability of the resulting PVP/MWCNT nanocomposite. Finally, we have prepared MWCNT/fiber mats with improved mechanical properties. These membranes, despite their fragility, exhibit a significant increase in their elastic modulus ($\sim 250\%$) for a low MWCNT load (≈ 0.01 wt.%), i.e., are a reinforced composite. These properties may be exploited in many industrial and bio-applications, e.g., water/soil/air remediation, where organic-organic mats based on nanocarbon are desired. Our results provide both a roadmap and proof of concept for the design of next-generation organic-organic nanocomposites via electrospinning.

ASSOCIATED CONTENT

Supporting Information

The Supporting Information is available free of charge on the ACS Publications website at DOI: 10.1021/acs.jpcc.xxxxxxxx.

XRD, SEM, TEM, photographs of samples and the experimental setup for mechanical measurements, electrospinning parameters for microparticle and fiber preparation, and viscosity versus shear rate data

AUTHOR INFORMATION

Corresponding Author

*E-mail (C. P. Narvaez-Muñoz): cpnarvaez1@espe.edu.ec.

*E-mail (C. Zamora-Ledezma): czamora@yachaytech.edu.ec.

Author Contributions

C.P.N.-M., L.M.C.-M.. and C.Z.-L., designed, performed, and supervised the research; C.P.N.-M. and L.M.C.-M. contributed with rheological and mechanical tests; K.S.V., A.D. and C.R.A. contributed with SEM/TEM measurements/statistical analysis; C.E.A.-N. and V.G. contributed with the Raman measurement/analysis; V.M.F. contributed with the DRX, SEM, TEM measurements and mechanical analysis; D.J.M. contributed with DFT calculations and theoretical modeling; and C.P.N.-M., C.R.A., D.J.M., and C.Z.-L. analyzed the data and wrote the paper.

Notes

The authors declare no competing financial interest.

ACKNOWLEDGMENTS

This work was partially supported by the research project PIC-16-BENS-002, ENSAMBLE scholarship program of the SENESCYT, and employed the Imbabura cluster of Yachay Tech University, which was purchased under contract No. 2017-024 (SIE-UITEY-007-2017). V.M-F. thanks the the VI-PPIT-Universidad de Sevilla for financial support. The authors thank Andrea Vanessa Vaca Mora for her assistance during SEM observations.

REFERENCES

(1) Han, J.; Xiong, L.; Jiang, X.; Yuan, X.; Zhao, Y.; Yang, D. Bio-functional electrospun nanomaterials: From topology design to biological applications. *Progress in Polymer Science* **2019**, *91*, 1–28.

(2) Xue, J.; Xie, J.; Liu, W.; Xia, Y. Electrospun Nanofibers: New Concepts, Materials, and Applications. *Accounts of Chemical Research* **2017**, *50*, 1976–1987.

(3) Haaf, F.; Sanner, A.; Straub, F. Polymers of N-Vinylpyrrolidone: Synthesis, Characterization and Uses. *Polymer Journal* **1985**, *17*, 143.

(4) Ma, P.-C.; Siddiqui, N. A.; Marom, G.; Kim, J.-K. Dispersion and functionalization of carbon nanotubes for polymer-based nanocomposites: A review. *Composites Part A* **2010**, *41*, 1345–1367.

(5) Sherlala, A. I. A.; Raman, A. A. A.; Bello, M.; Asghar, A. A review of the applications of organo-functionalized magnetic graphene oxide nanocomposites for heavy metal adsorption. *Chemosphere* **2018**, *193*, 1004.

(6) Torres-Canas, F.; Blanc, C.; Mašlík, J.; Tahir, S.; Izard, N.; Karasahin, S.; Castellani, M.; Dammasch, M.; Zamora-Ledezma, C.; Anglaret, E. Morphology and anisotropy of thin conductive inkjet printed lines of single-walled carbon nanotubes. *Materials Research Express* **2017**, *4*, 035037.

(7) Torres-Canas, F. J.; Blanc, C.; Zamora-Ledezma, C.; Silva, P.; Anglaret, E. Dispersion and Individualization of SWNT in Surfactant-Free Suspensions and Composites of Hydrosoluble Polymers. *The Journal of Physical Chemistry C* **2015**, *119*, 703–709.

(8) Zamora-Ledezma, C.; Buisson, L.; Moulton, S. E.; Wallace, G.; Zakri, C.; Blanc, C.; Anglaret, E.; Poulin, P. Carbon Nanotubes Induced Gelation of Unmodified Hyaluronic Acid. *Langmuir* **2013**, *29*, 10247–10253.

(9) Zamora-Ledezma, C.; Añez, L.; Primera, J.; Silva, P.; Etienne-Calas, S.; Anglaret, E. Photoluminescent single wall carbon nanotube–silica composite gels. *Carbon* **2008**, *46*, 1253–1255.

(10) Esquivias, L.; Rivero-Antúnez, P.; Zamora-Ledezma, C.; Domínguez-Rodríguez, A.; Morales-Flórez, V. Intragranular carbon nanotubes in alumina-based composites for reinforced ceramics. *Journal of Sol-Gel Science and Technology* **2018**, 162–171.

(11) Dresselhaus, M. S., Dresselhaus, G., Avouris, P., Eds. *Carbon Nanotubes: Synthesis, Structure, Properties, and Applications*; Springer-Verlag Berlin Heidelberg, 2001.

(12) Teo, W. E.; Ramakrishna, S. A review on electrospinning design and nanofibre assemblies. *Nanotechnology* **2006**, *17*, R89–R106.

(13) Mei, L.-Y.; Song, P.; Liu, Y.-Q. Magnetic-field-assisted electrospinning highly aligned composite nanofibers containing well-aligned multiwalled carbon nanotubes. *Journal of Applied Polymer Science* **2015**, *132*, 41995.

(14) He, J.-H.; Kong, H.-Y.; Yang, R.-R.; Dou, H.; Faraz, N.; Wand, L.; Feng, C. Review on Fiber Morphology Obtained by Bubble Electrospinning and Blown Bubble Spinning. *Thermal Science* **2012**, *16*, 1263–1279.

(15) Cloupeau, M.; Prunet-Foch, B. Electrohydrodynamic spraying functioning modes: a critical review. *Journal of Aerosol Science* **1994**, *25*, 1021–1036.

(16) Vongsetskul, T.; Chantarodsakun, T.; Wongsomboon, P.; Rangk, R. Effect of Solvent and Processing Parameters on Electrospun Polyvinylpyrrolidone Ultra-fine Fibers. *Chiang Mai Journal of Science* **2015**, *42*, 436–442.

(17) Schneider, C. A.; Rasband, W. S.; Eliceiri, K. W. NIHf Image to ImageJ. *Nature Methods* **2012**, *9*, 671–675.

(18) Larsen, A. H.; Vanin, M.; Mortensen, J. J.; Thygesen, K. S.; Jacobsen, K. W. Localized Atomic Basis Set in the Projector Augmented Wave Method. *Phys. Rev. B: Condens. Matter Mater. Phys.* **2009**, *80*, 195112.
(19) Mortensen, J. J.; Hansen, L. B.; Jacobsen, K. W. Real-Space Grid Implementation of the Projector Augmented Wave Method. *Phys. Rev. B: Condens. Matter Mater. Phys.* **2005**, *71*, 035109.
(20) Enkovaara, J.; Rostgaard, C.; Mortensen, J. J.; Chen, J.; Dułak, M.; Ferrighi, L.; Gavnholt, J.; Glinsvad, C.; Haikola, V.; Hansen, H. A.; Kristoffersen, H. H.; Kuisma, M.; Larsen, A. H.; Lehtovaara, L.; Ljungberg, M.; Lopez-Acevedo, O.; Moses, P. G.; Ojanen, J.; Olsen, T.; Petzold, V.; Romero, N. A.; Stausholm-Møller, J.; Strange, M.; Tritsaris, G. A.; Vanin, M.; Walter, M.; Hammer, B.; Häkkinen, H.; Madsen, G. K. H.; Nieminen, R. M.; Nørskov, J. K.; Puska, M.; Rantala, T. T.; Schiøtz, J.; Thygesen, K. S.; Jacobsen, K. W. Electronic Structure Calculations with GPAW: A Real-Space Implementation of the Projector Augmented-Wave Method. *J. Phys.: Condens. Matter* **2010**, *22*, 253202.
(21) Perdew, J. P.; Burke, K.; Ernzerhof, M. Generalized Gradient Approximation Made Simple. *Phys. Rev. Lett.* **1996**, *77*, 3865.
(22) Bader, R. F. W. *Atoms in Molecules: A Quantum Theory*; Oxford University, 1990; Vol. 3; pp 1–120.
(23) Atkins, P.; de Paula, J. *Physical Chemistry*, 8th ed.; Oxford University Press: London, 2006.
(24) García-Lastra, J. M.; Mowbray, D. J.; Thygesen, K. S.; Rubio, A.; Jacobsen, K. W. Modeling nanoscale gas sensors under realistic conditions: Computational screening of metal-doped carbon nanotubes. *Physical Review B* **2010**, *81*, 245429.
(25) Mowbray, D. J.; Garca-Lastra, J. M.; Thygesen, K. S.; Rubio, A.; Jacobsen, K. W. Designing multifunctional chemical sensors using Ni and Cu doped carbon nanotubes. *physica status solidi (b)* **2010**, *247*, 2678–2682.
(26) Deitzel, J.; Kleinmeyer, J.; Harris, D.; Tan, N. B. The effect of processing variables on the morphology of electrospun nanofibers and textiles. *Polymer* **2001**, *42*, 261–272.
(27) Omran Alkhayatt1, A. H.; Al-Azzawi, A. H.; Alakayashi, Z. Rheological and optical characterization of Polyvinylpyrrolidone (PVP) - Polyethylene glycol (PEG) polymer blends. *IOSR Journal of Applied Physics* **2016**, *8*, 2278–4861.
(28) Marani, D.; Sudireddy, B. R.; Kiebach, R.; Nielsen, L.; Ndoni, S. *Nordic Rheology Society Annual Transactions*; Nordic Rheology Society: Reyjavik, Iceland, 2014; Vol. 22.
(29) Pillay, V.; Dott, C.; Choonara, Y. E.; Tyagi, C.; Tomar, L.; Kumar, P.; du Toit, L. C.; Ndesendo, V. M. K. A Review of the Effect of Processing Variables on the Fabrication of Electrospun Nanofibers for Drug Delivery Applications. *Journal of Nanomaterials* **2013**, *2013*, 789289.
(30) Munir, M. M.; Suryamas, A. B.; Iskandar, F.; Okuyama, K. Scaling law on particle-to-fiber formation during electrospinning. *Polymer* **2009**, *50*, 4935–4943.
(31) Lehman, J. H.; Terrones, M.; Mansfield, E.; Hurst, K. E.; Meunier, V. Evaluating the characteristics of multiwall carbon nanotubes. *Carbon* **2011**, *49*, 2581–2602.
(32) Mao, H.; Feng, J.; Ma, X.; Wu, C.; Zhao, X. One-dimensional silver nanowires synthesized by self-seeding polyol process. *Journal of Nanoparticle Research* **2012**, *14*, 887.
(33) Fini, A.; Cavallari, C.; Ospitali, F. Raman and thermal analysis of indomethacin/PVP solid dispersion enteric microparticles. *European Journal of Pharmaceutics and Biopharmaceutics* **2008**, *70*, 409–420.
(34) Zamora-Ledezma, C.; Blanc, C.; Anglaret, E. Controlled Alignment of Individual Single-Wall Carbon Nanotubes at High Concentrations in Polymer Matrices. *The Journal of Physical Chemistry C* **2012**, *116*, 13760–13766.
(35) Andrews, R.; Weisenberger, M. Carbon nanotube polymer composites. *Current Opinion in Solid State and Materials Science* **2004**, *8*, 31–37.
(36) Bazbouz, M. B.; Stylios, G. K. The tensile properties of electrospun nylon 6 single nanofibers. *Journal of Polymer Science Part B: Polymer Physics* **2010**, *48*, 1719–1731.

Graphical TOC Entry